

## 3D-Printed Mechanochromic Materials

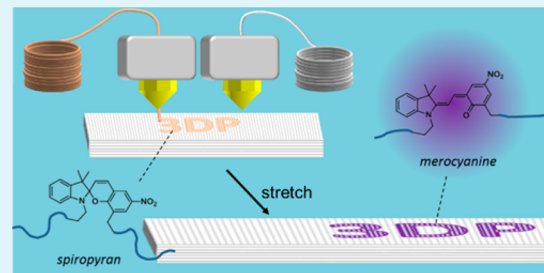
Gregory I. Peterson,<sup>†</sup> Michael B. Larsen,<sup>†</sup> Mark A. Ganter,<sup>‡</sup> Duane W. Storti,<sup>‡</sup> and Andrew J. Boydston\*,<sup>†</sup>

<sup>†</sup>Department of Chemistry and <sup>‡</sup>Department of Mechanical Engineering, University of Washington, Seattle, Washington 98195 United States

### Supporting Information

**ABSTRACT:** We describe the preparation and characterization of photo- and mechanochromic 3D-printed structures using a commercial fused filament fabrication printer. Three spiroxanthene-containing poly( $\epsilon$ -caprolactone) (PCL) polymers were each filamentized and used to print single- and multicomponent tensile testing specimens that would be difficult, if not impossible, to prepare using traditional manufacturing techniques. It was determined that the filament production and printing process did not degrade the spiroxanthene units or polymer chains and that the mechanical properties of the specimens prepared with the custom filament were in good agreement with those from commercial PCL filament. In addition to printing photochromic and dual photo- and mechanochromic PCL materials, we also prepare PCL containing a spiroxanthene unit that is selectively activated by mechanical impetus. Multicomponent specimens containing two different responsive spiroxanthenes enabled selective activation of different regions within the specimen depending on the stimulus applied to the material. By taking advantage of the unique capabilities of 3D printing, we also demonstrate rapid modification of a prototype force sensor that enables the assessment of peak load by simple visual assessment of mechanochromism.

**KEYWORDS:** additive manufacturing, mechanochemistry, polymers, responsive materials



### INTRODUCTION

Three-dimensional printing (3DP) is a method of additive manufacturing that enables the construction of 3D objects based upon a digital model. Although the basic methods for 3DP have been known for decades, the area has seen a recent surge of interest as researchers continue to develop new materials that enhance the capabilities of 3DP and as broader communities find new applications that benefit from software-reconfigurable rapid prototyping.<sup>1–3</sup> When a digital model is supplied to the printer, the printing system uses slicing software that converts the 3D model to 2D slice descriptions, and a G-code generator converts the slice descriptions into numerically controlled machine instructions. With this approach to manufacturing, the time and resources required for production of a single prototype of an envisioned object are streamlined. In contrast to traditional manufacturing techniques, such as injection or compression molding, the advantages of 3DP include increased customizability, ease of use, orthogonality to existing manufacturing techniques, and access to the technique by a wide user base of a variety of backgrounds and skill levels. Fused filament fabrication (FFF), for instance, has become accessible in private homes for printing the likes of toys, housewares, art pieces, and accessories for portable electronics.

An exciting and potentially transformative area of growth is the integration of functional polymeric materials with 3DP technologies.<sup>1,2</sup> As these areas merge, the capabilities afforded by designer polymer synthesis can be incorporated into rapidly customizable objects and devices.<sup>4,5</sup> Examples of 3D-printed functional materials and devices include drug delivery plat-

forms,<sup>6,7</sup> tissue scaffolds,<sup>8–11</sup> energy storage devices,<sup>12,13</sup> electrically conductive materials,<sup>14–17</sup> and force-sensors.<sup>18–20</sup>

We envisioned the ability to incorporate mechanochemically responsive units into materials amenable to 3DP techniques to produce printed objects with well-defined shapes and regions capable of chemo-mechanical coupling.<sup>20</sup> Recent advances in polymer mechanochemistry have given rise to systems that translate macroscopic mechanical force into specific chemical reactivity.<sup>21–24</sup> In the solid state, mechano-responsive polymers and materials have shown promise for applications including mechanochromic force sensors,<sup>25–32</sup> mechano-catalysis,<sup>33</sup> self-reinforcing materials,<sup>33,34</sup> and scaffolds for small molecule release.<sup>25,35–37</sup> Among the various mechanophores reported in the literature, we were particularly interested in the mechanochromic spiroxanthene systems that have been extensively studied in the field, as the ease of determining qualitative activation in this system is unmatched.<sup>25–30</sup> Upon application of force across the C<sub>spiro</sub>-O bond (Figure 1), isomerization of the spiroxanthene to its highly colored purple merocyanine isomer can be accomplished, effectively enabling the self-reporting of stress accumulation within a macroscopic material via readily identifiable color change.

Recently, we demonstrated the 3DP of poly( $\epsilon$ -caprolactone) (PCL) containing a chain-centered spiroxanthene and explored its basic mechano-responsive characteristics in a notched specimen and prototype force sensor.<sup>20</sup> In this manuscript, we character-

Received: October 1, 2014

Accepted: December 5, 2014

Published: December 5, 2014



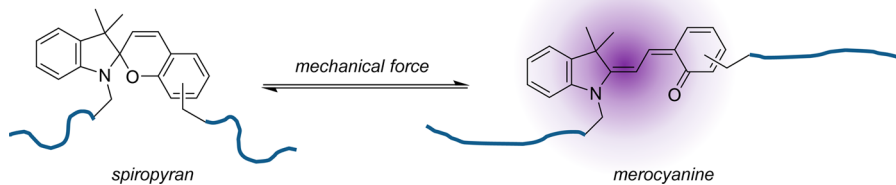


**Figure 1.** Generalized depiction of the mechanochemical isomerization of a spiropyran moiety to its merocyanine form.

ize the mechanical properties of the printed materials and explore the extent to which polymer degradation occurs during filament formation and extrusion printing. We also examine the incorporation of different spiropyran moieties into 3D printed PCL. Specifically, we prepare multicomponent specimens that display selective activation of specific regions in the materials, depending on the stimulus being applied. These results include the first demonstration of a spiropyran that is uniquely responsive to mechanical force without displaying the same photoresponsiveness observed from all previously reported spiropyran mechanophores. We also showcase the unique abilities of 3DP in contrast with other traditional manufacturing techniques by demonstrating rapid customization of the dynamic sensing range of a force sensor. The utility of this paradigm and its suitability for broad adoption is supported by presenting illustrative results obtained using only inexpensive entry-level 3DP technology and freely available software.

## EXPERIMENTAL SECTION

**Materials.** Dry toluene was obtained from a Glass Contour solvent purification system. The monomer  $\epsilon$ -caprolactone was dried over 4 Å molecular sieves for 48 h prior to use. House N<sub>2</sub> was passed through a drying tube before use. All other reagents and solvents were used as obtained from commercial sources.

**Characterization.** See the Supporting Information for gel permeation chromatography (GPC) traces, NMR spectra, UV-vis spectra, and descriptions of analytical instrumentation.

**Synthesis of Polymer 3.** Initiator **1** and polymer **3** were prepared following a reported procedure.<sup>29</sup>

**Synthesis of Polymer 4.** A flame-dried and N<sub>2</sub>-purged three-neck round-bottom flask fitted with a reflux condenser was charged with initiator **2** (prepared as previously reported,<sup>38</sup> 268 mg, 0.76 mmol, 1.0 mol equiv) and a stir bar. To the reaction flask was then added  $\epsilon$ -caprolactone (29.4 mL, 265 mmol, 350 mol equiv) and dry toluene (30.0 mL). Finally, Sn(Oct)<sub>2</sub> (80  $\mu$ L, 0.251 mmol, 0.33 mol equiv) was added and the reaction solution was brought to refluxing temperature. After 24 h, the reaction solution was brought to 40 °C, diluted with toluene (~150 mL), and stirred until the polymer was fully dissolved. The polymer solution was then precipitated into an excess of cold MeOH, after which the precipitate was collected via vacuum filtration and then dried under reduced pressure. The PCL product was obtained as a brown solid in 96% yield (29.0 g).

**Synthesis of Initiator 7.** Indole **5** (prepared as previously reported,<sup>29</sup> 266 mg, 1.31 mmol, 1.0 mol equiv) and salicylaldehyde **6** (prepared as previously reported,<sup>39</sup> 200 mg, 1.31 mmol, 1.0 mol equiv) were dissolved in 5 mL of absolute ethanol. Piperidine (0.26 mL, 2.63 mmol, 2.0 mol equiv) was added and the solution brought to reflux. After 6 h the reaction was judged to be complete by TLC. The reaction was cooled to room temperature and diluted with 20 mL of ethyl acetate and washed successively with water (3  $\times$  20 mL) and brine (1  $\times$  10 mL). The organic layer was dried over MgSO<sub>4</sub> and concentrated under reduced pressure to yield **7** as a black crystalline solid in 91% yield (401 mg). <sup>1</sup>H NMR (300 MHz, CDCl<sub>3</sub>)  $\delta$  7.17 (td, *J* = 7.7, 1.3 Hz, 1H), 7.11–7.05 (m, 3H), 6.86 (td, *J* = 7.4, 0.8 Hz, 1H), 6.83 (d, *J* = 10.2 Hz, 1H), 6.68 (d, *J* = 7.9 Hz, 1H), 6.63 (d, *J* = 7.8 Hz, 1H), 5.69 (d, *J* = 10.2 Hz, 1H), 4.57 (s, 2H), 3.79–3.70 (m, 2H),

3.56–3.45 (m, 1H), 3.40–3.26 (m, 1H), 1.30 (s, 3H), 1.17 (s, 3H). <sup>13</sup>C NMR (126 MHz, CDCl<sub>3</sub>)  $\delta$  153.5, 147.3, 136.3, 132.9, 129.3, 129.0, 127.6, 125.9, 121.8, 119.9, 119.3, 118.6, 115.1, 106.6, 104.7, 64.9, 60.8, 52.3, 46.0, 25.8, 20.3. MS (ESI): [M + H]<sup>+</sup> calculated for C<sub>21</sub>H<sub>24</sub>NO<sub>3</sub>, 338.18; found, 338.4.

**Synthesis of Polymer 8.** Polymer **8** was prepared in the same manner as described in Synthesis of Polymer **4**, except **7** was used as an initiator (**7** = 164 mg, 0.49 mmol;  $\epsilon$ -caprolactone = 18.84 mL, 170.1 mmol, 350 mol equiv.; toluene = 20 mL; Sn(Oct)<sub>2</sub> = 0.05 mL, 0.16 mmol, 0.33 mol equiv). The polymer was obtained in 96% yield (18.7 g).

**Filament Production.** Polymers **3** and **4** were mixed with Makerbot Flexible Filament (C) cut into small pieces, melted with a heat gun, and manually mixed with a spatula. After cooling, the resulting solid mixture was cut into small pieces with scissors and put into an electronically controlled burr mill with dry ice. The polymer was ground into particles no larger than 5 mm in diameter and then made into filament via melt extrusion (at 63 °C) with a Filabot Wee filament extruder. The filament **3**<sub>100</sub> was produced without blending in any commercial filament C.

**3D Printing.** 3D structures were designed and converted to STL files using Sketchup 2013 computer aided design (CAD) software. The STL files were imported into Replicator G (version 0040) and G-code (for Makerbot class machines) was generated using either Slic3r 0.X (for single material prints) or Skeinforge 50 (for multimaterial prints) slicing programs. Multimaterial prints required the generation of G-code for each component individually, followed by their merger using Replicator G. A Flashforge Creator dual-head FFF 3D printer (firmware 7.2) was used to read the G-code and print the 3D object. Objects were printed centered on a nonheated Plexiglas build plate with the long axis of the specimen aligned with the y axis of the build plate (build space axes shown in Figure S1, Supporting Information). Objects were built up in the vertical z axis (as indicated for all parts in the Supporting Information). The outline of the specimen was printed first with its thickness depending on the number of shells. For the first layer, the extruded polymer was laid in alignment with the y axis. For the second, the polymer was laid in alignment with the x axis. The fill alignment continually alternates such that the layers above or below any one layer are perpendicular to each other. Extrusion nozzles were heated to 110 °C (filament was more prone to jamming at lower temperatures). Additional print parameters included print speeds set to 20 mm/s, travel speed set to 50 mm/s, retraction disabled when applicable (i.e., when using Slic3r), two shells, fill density of 1 (i.e., 100% fill), and layer height of 0.25 mm. To ensure the most accurate filament diameter, each sample of filament was measured with calipers in multiple places along the section to be used for printing and the average diameter was used in the print parameters. Dimensions of each printed specimen are provided in the Supporting Information.

**Mechanical Testing.** Tensile testing of printed specimens was performed on an Instron 5500R load frame with a 5 kN load cell controlled using Bluehill 3.0 software. All tests were conducted using a crosshead rate of 100 mm/min. Dimensions of each specimen were measured with calipers prior to testing to ensure accurate calculation of stress and strain for each sample. Three specimens were tested for a given filament type.

## RESULTS AND DISCUSSION

Three spiropyran containing polymers were prepared via ring opening polymerization of  $\epsilon$ -caprolactone from spiropyran alcohol initiators (Scheme 1). Polymers 3 ( $M_w = 90.0$  kDa,  $D = 1.16$ ) and 8 ( $M_w = 82.5$  kDa,  $D = 1.18$ ) bear chain-centered spiropyrans such that elongation of the polymer results in stress accumulation across the desired C<sub>spiro</sub>-O bond, and isomerization is activated. In contrast, polymer 4 ( $M_w = 64.9$  kDa,  $D = 1.43$ ) has a chain-end spiropyran moiety such that stress will not be accumulated across the necessary bond, and thus, it should not be activated by mechanical stimulus. Notably, each of these polymers is of sufficient molecular weight to accumulate tensile forces within the main chain that are great enough to induce mechanochemical activation.

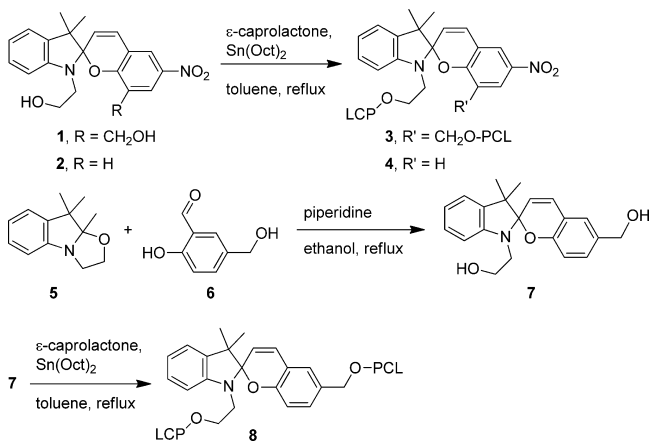
Each polymer was blended with commercial PCL (C) at various concentrations (Table 1). The wt % of each spiropyran

**Table 1. Structure, Molecular Weight, and Dispersity Data for the Synthesized and Commercial Polymer and Compositions of Various Filament Types**

filament	polymer	$M_w$ (kDa), D	blend	spiropyran % (w/w)
3 <sub>10</sub>	3	90.0, 1.16	10% w/w with C	0.05
3 <sub>50</sub>			50% w/w with C	0.25
3 <sub>100</sub>			none	0.50
4 <sub>50</sub>	4	64.9, 1.43	50% w/w with C	0.39
8 <sub>50</sub>	8	82.5, 1.18	50% w/w with C	0.43
C <sub>100</sub>	C	62.7, 1.29	none	none

containing polymer is denoted by the subscript (e.g., 3<sub>10</sub> is comprised of 10 wt % 3 and 90 wt % C). Filament was prepared using a single screw melt extruder. Average batch-to-batch filament diameters ranged from ca. 1.55 to 1.85 mm, with variation along the filament typically being less than  $\pm 0.05$  mm. The custom filaments were used to print tensile testing specimens using a commercial dual-extrusion head FFF printer. Printing was initially performed using only one of the extrusion heads set at a temperature of 110 °C, a nonheated build plate, and a relatively slow print speed of 20 mm/s (in comparison with 120–150 mm/s typically used for printing acrylonitrile-butadiene-styrene or poly(lactic acid) filament). Due to the relatively flexible nature of the filament, retraction was disabled to avoid jamming of the filament during printing.

**Scheme 1. Synthesis of Polymers 3, 4, and 8**



During the mixing and melt extrusion steps of the filament formation process, no color changes were observed from any of the spiropyran-containing materials. Additionally, no color changes were observed during printing, indicating no thermal activation of the spiropyran was taking place. To determine if any polymer degradation was occurring during the preprint processing or printing, a printed specimen was subjected to GPC analysis. No detectable changes in polymer molecular weight or dispersity were observed as compared to the virgin polymer (Figure 2).

During the mixing and melt extrusion steps of the filament formation process, no color changes were observed from any of the spiropyran-containing materials. Additionally, no color changes were observed during printing, indicating no thermal activation of the spiropyran was taking place. To determine if any polymer degradation was occurring during the preprint processing or printing, a printed specimen was subjected to GPC analysis. No detectable changes in polymer molecular weight or dispersity were observed as compared to the virgin polymer (Figure 2).

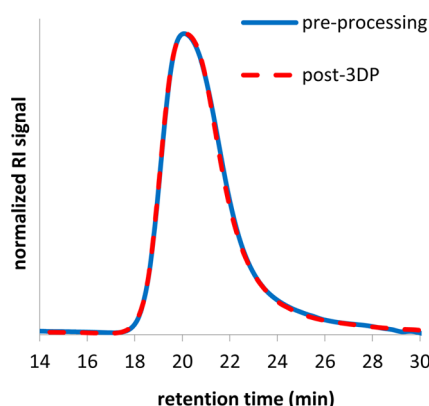


**Figure 2.** GPC chromatograms of polymer 3 prior to any filament or print processing and after 3DP.

To examine the basic mechanochemical reactivity and mechanical properties of the materials and to ensure a controlled environment for elongation, tensile testing of “dog bone” shaped specimens was performed on an Instron load frame. In all cases in which 3 was present, color change from brown to purple was observed upon elongation and necking of the sample, signifying mechanochemical activation of the spiropyran in accordance with previous studies.<sup>25–30</sup> While the intensity of the resulting color was directly related to the amount of 3 used in the blend (Figure 3), the most apparent

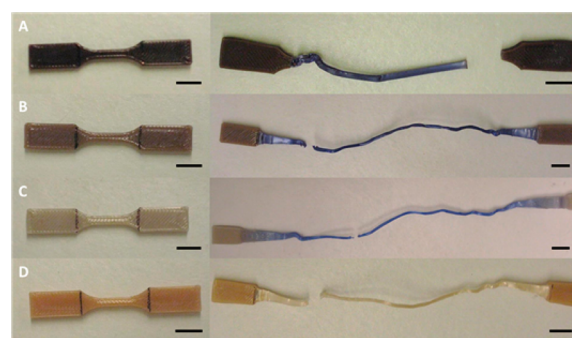


**Figure 3.** Tensile test specimens made from (A) 3<sub>100</sub>, (B) 3<sub>50</sub>, (C) 3<sub>10</sub>, and (D) 4<sub>50</sub> pre- and postelongation. The vertical marks on the specimen indicate the position of the load frame clamps. Scale bars = 10 mm.

contrast between virgin and elongated (activated) materials was observed for blends having lower loading of spiropyran, due to the lighter color of the unactivated material. No spiropyran activation was observed in the test specimens made from 4<sub>50</sub> in which the mechanophore is located at a chain end, thus confirming the mechanical origin of the color change. Although the Young's modulus and yield strength of each blended

**Table 2. Summary of the Materials Properties of the Test Specimens Prepared from the Various Filament Types<sup>a</sup>**

filament type	modulus (GPa)	yield strength (MPa)	tensile strength (MPa)	percent elongation to break
C <sub>100</sub>	0.336 ± 0.042	16.57 ± 0.20	33.24 ± 1.15	709 ± 25
C <sub>100</sub> (re-extruded)	0.225 ± 0.011	13.3 ± 0.10	n. d. <sup>b</sup>	n. d. <sup>b</sup>
3 <sub>40</sub>	0.268 ± 0.029	13.32 ± 0.42	29.50 ± 1.12	750 ± 81
3 <sub>50</sub>	0.300 ± 0.003	14.56 ± 0.48	27.17 ± 1.94	664 ± 37
3 <sub>100</sub>	0.351 ± 0.030	17.49 ± 0.24	14.86 ± 1.71	302 ± 12
4 <sub>50</sub>	0.300 ± 0.067	15.00 ± 0.21	26.82 ± 0.31	651 ± 12
3 <sub>50</sub> encased in C <sub>100</sub>	0.308 ± 0.045	15.96 ± 0.83	33.15 ± 1.61	716 ± 56

<sup>a</sup>Values are an average of three experiments ± 1 standard deviation. <sup>b</sup>Not determined since the samples necked into the grip region and slipped from the grips in all samples measured.

material were found to be lower than that of the nonblends (Table 2), all are in good agreement with reported values for PCL.<sup>40</sup> Refilamentizing the commercial material C also led to a decrease in Young's modulus and yield strength. As GPC analysis showed no polymer degradation occurring during the processing/printing process (*vide supra*), a possible explanation in the differences of materials properties between C<sub>100</sub> and re-extruded C<sub>100</sub> could be the variation in diameter of the filament made in-house, leading to heterogeneity in the structure of the printed objects.

We next prepared multicomponent specimens that highlight the capabilities of 3DP in contrast with other types of traditional manufacturing methods, such as injection or compression molding. A tensile test specimen comprising discrete regions of photo- and mechano-responsive 3<sub>50</sub> and photoresponsive 4<sub>50</sub> was printed in a single session by using two extrusion heads, each loaded with one of the filament types. In this particular dual extrusion technique, the active print head alternates such that only one head is printing at a time. The test specimen body was comprised mainly of 4<sub>50</sub>, which was used as a housing around two surface channels of 3<sub>50</sub> that spanned the length of the printed specimen (Figure 4). Upon elongation of

We next considered a system in which the chromic response could be selectively activated with mechanical impetus. Absent the electron-withdrawing nitro functionality, the photostationary state of UV-irradiated spirobifluoranes contains a negligible amount of the corresponding merocyanine isomer, and thus, no photochromism is observed.<sup>41–43</sup> However, we found that application of stress across the C<sub>spiro</sub>—O bond still resulted in mechanochromism in this spirobifluorane. To demonstrate this in a 3D-printed specimen, we prepared a multicomponent specimen similar to the one depicted in Figure 4, but with a body composed of 8<sub>50</sub> (mechano-responsive but not photoresponsive), and the surface channels composed of 4<sub>50</sub>, (photoresponsive but not mechano-responsive; Figure 5A). Irradiation

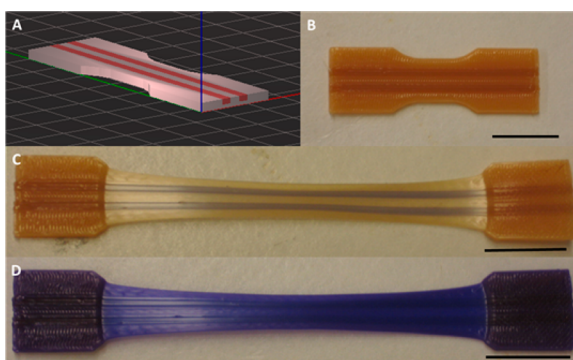


**Figure 4.** (A) CAD representation of a multicomponent tensile test specimen, with red stripes indicating the location of the mechano-responsive filament 3<sub>50</sub> (specimen body comprised of 4<sub>50</sub>), (B) test specimen pre-elongation, (C) test specimen postelongation showing the mechanochromic response of the 3<sub>50</sub> regions, and (D) test specimen postelongation after 365 nm UV irradiation showing activation of both the 3<sub>50</sub> and 4<sub>50</sub> regions. Scale bars = 20 mm.

the sample, only the regions containing 3<sub>50</sub> were activated, signifying the spatio-control over the material's response to external force. Notably, the spirobifluorane moieties in both materials were still susceptible to UV-triggered isomerization and confirmation of spirobifluorane content throughout the materials was confirmed upon illumination with 365 nm light from a hand-held UV lamp.

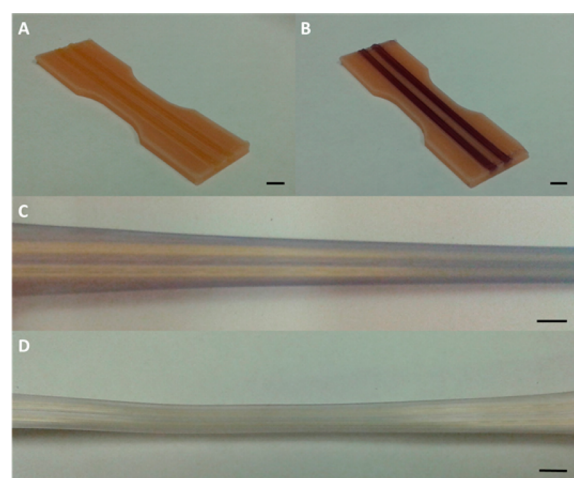


**Figure 5.** (A) Test specimen composed of 8<sub>50</sub> with stripes of 4<sub>50</sub>, (B) test specimen after 365 nm UV irradiation showing the photochromic response of the 4<sub>50</sub> regions, (C) test specimen under load in the load frame showing the mechanochromic response of the 8<sub>50</sub> regions, and (D) test specimen ca. 30 s after removal of load showing almost complete loss of the purple color in the 8<sub>50</sub> regions. Scale bars = 5 mm.

of the specimen with 365 nm UV radiation only led to activation of the regions containing 4<sub>50</sub> (Figure 5B). On the other hand, elongation of the specimen led to activation of the 8<sub>50</sub> regions but not of the 4<sub>50</sub> regions (Figure 5C), consistent with the results in Figure 4. Visually detectable activation of polymer 8 was only readily observed when the polymer was under load; upon relieving the tension on the specimen, the purple color rapidly disappeared. For example, within the ca. 30 s required to remove the sample from the grips in the load frame, nearly all of the purple color had disappeared (Figure 5D). The reactivity of polymer 8 is significant because it enables the use of these mechanochromic materials in outdoor applications, whereas polymers 3 and 4, which are both

photoresponsive, are rapidly converted to the merocyanine form in direct sunlight.

We next explored the use of 3DP to prepare objects in which a center region of mechano-responsive  $3_{50}$  was completely encased by  $C_{100}$  (Figure 6), a type of structure that would be

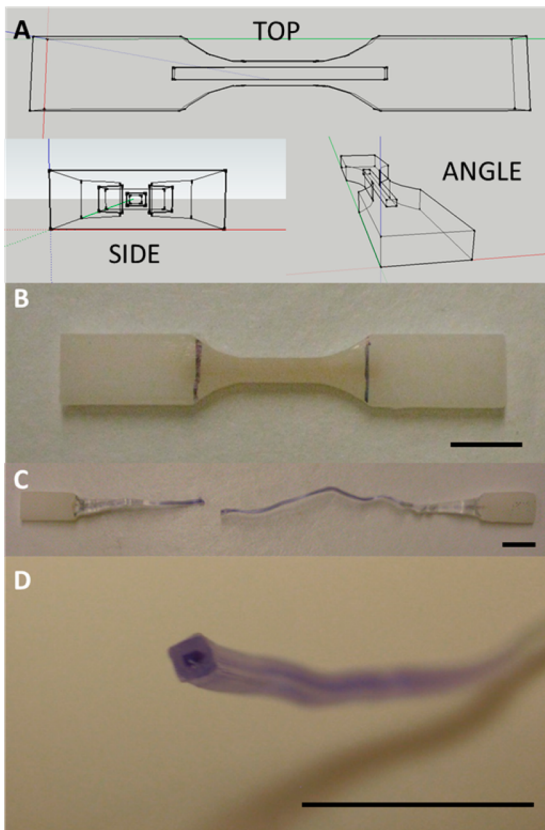


**Figure 6.** (A) CAD representations of the tensile test specimen in which the mechano-responsive region is encased by nonmechano-responsive filament, (B) test specimen in which  $3_{50}$  is encased by  $C_{100}$  (the vertical lines on the specimen indicate the position of the load frame clamps), (C) test specimen postelongation showing the mechanochromism of the  $3_{50}$  region, and (D) elongated and cut specimen showing the encased filament. Scale bars = 10 mm.

difficult (if not impossible) to prepare in a single operation via most other manufacturing techniques. Using the dual extrusion method, the target configuration was printed in a single session and then subjected to elongation as before. The  $3_{50}$  region was again activated and the color change was visible from the exterior of the material. The mechanical properties of this specimen design were similar to the specimens comprised solely of C (Table 2), indicating that the stimuli-responsive properties of  $3_{50}$  can be imparted to larger prints without affecting the bulk properties of the material. Using the same print code and replacing C with control filament  $4_{50}$  as the exterior material resulted in a sample in which the  $3_{50}$  region was not visible prior to elongation (Figure 7). Upon tensile testing, the mechano-responsive core became clearly distinguishable from the encasing filament.

Prototype force sensors were developed to demonstrate the potential engineering applications that can be accessed by integrating mechano-responsive polymers and 3DP technology. An asymmetric tensile test specimen was prepared with multiple embedded regions of  $3_{50}$  spaced evenly within the

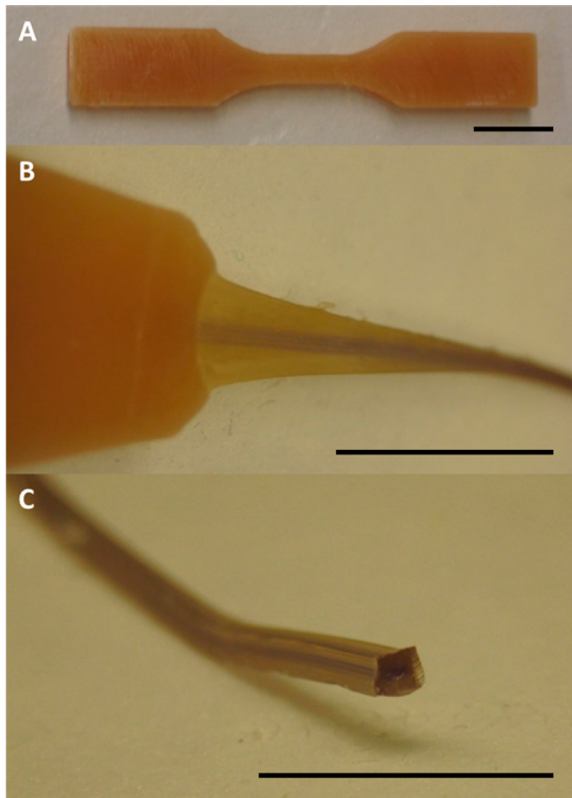


**Figure 7.** (A) Tensile test specimen in which  $3_{50}$  is encased by  $4_{50}$ , (B) test specimen postelongation showing the mechanochromism of the  $3_{50}$  region, and (C) elongated and cut specimen showing the encased filament. Scale bars = 10 mm.

gauge section (Figure 8). Initial testing of dog bones with constant cross section produced force–extension curves that

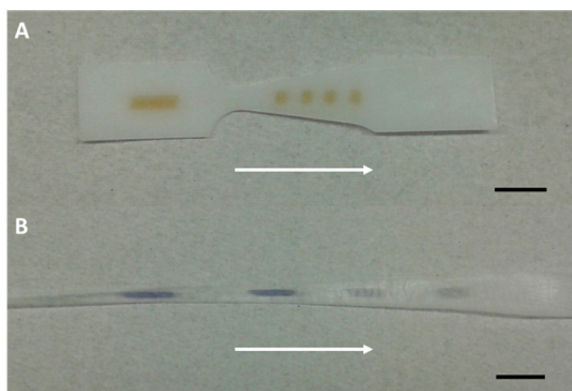


**Figure 8.** (A) 1 mm thick force sensor before elongation, and (B) postelongation. The white arrows indicate the direction of necking. Scale bars = 10 mm.

were flat between initial necking and eventual strain hardening (Figure S2, Supporting Information). This led us to pursue an asymmetric dog bone with a variable cross section. Introducing a section width that varies linearly with displacement along the axis of symmetry resulted in a relationship between the extension and the force required to draw the material that is linear over a broad domain of extension. By controlling the initial location and direction in which the material necks, the design ensures sequential and predictable activation of each

mechano-responsive region (Figure S3, Supporting Information). The onset of activation of each region is directly related to a specific force that was applied to the specimen (Figure 9).

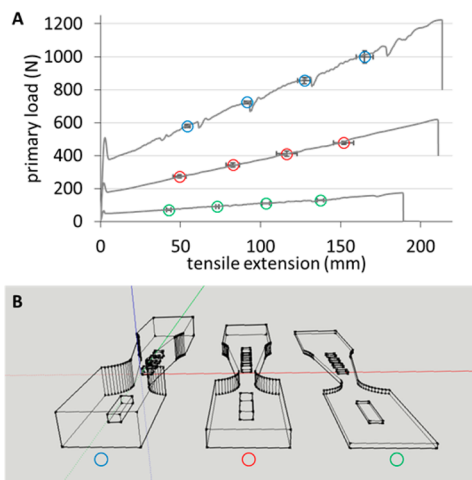


**Figure 9.** (A) Representative plots of tensile extension vs load for force sensors of ca. (green ○) 1, (red ○) 4, and (blue ○) 7 mm thickness. The markers indicate the onset of the activation of each mechano-responsive region (average of three runs). Error bars represent  $\pm 1$  standard deviation. (B) CAD representation of each of the force sensors.

By simply counting the number of activated regions, the amount of peak force applied to the material could be quickly estimated with no additional characterization or analysis. Good reproducibility of the force required to activate each region in the sensor is highlighted by the small standard deviations obtained after three test runs (Table S1, Supporting Information).

One advantage of using 3DP to prepare prototypes and end-user products is the ability to quickly modify and optimize designs for a given application. To demonstrate the ease with which this can be accomplished, we modified the thickness of our force sensor to expand the range of detectable loads. By simply changing the thickness dimension in our CAD design, we could quickly print different variations of the sensor without any additional tooling. In contrast, a similar process via injection molding would require preparation of a new mold for each design. By changing the thickness of the specimens, different dynamic ranges were able to be accessed. Specifically, increasing the specimen thickness from 1 to 7 mm led to nearly an order of magnitude increase in the forces detectable by the sensor. Furthermore, the number, shape, spacing, and composition of mechano-responsive regions could also be customized based on the needs of the application. Obtaining this level of customizability would be extremely difficult without using 3DP technologies.

## CONCLUSION

In summary, we have demonstrated the successful 3DP of a variety of stimuli-responsive polymers and the development of a new spiropyran mechanophore that exhibits selectivity toward mechanical activation by not exhibiting a photochromic response to either natural sunlight or 365 nm UV irradiation. The basic mechanical properties of the different structures prepared with various filament formulations showed some variation, but were within the range of reported values for PCL.

The use of 3DP enabled rapid production of multicomponent materials such as encased mechano-responsive materials within commercial or control polymers. These materials would generally be difficult or impossible to prepare with other manufacturing techniques. Additionally, rapid modification of a prototype force sensor was demonstrated to show its tunability and the advantages of using 3DP. These demonstrations were borne through the integration of mechano-responsive polymer technology and the unique features of 3DP. The ability to produce these materials using consumer level equipment is expected to facilitate adoption, use, and exploration by a wide audience.

## ASSOCIATED CONTENT

### S Supporting Information

Descriptions of analytical instruments, supplementary figures, specimen dimensions, and materials characterization. This material is available free of charge via the Internet at <http://pubs.acs.org>.

## AUTHOR INFORMATION

### Corresponding Author

\*E-mail: boydston@chem.washington.edu.

### Author Contributions

The manuscript was written through contributions of all authors. All authors have given approval to the final version of the manuscript.

### Notes

The authors declare no competing financial interest.

## ACKNOWLEDGMENTS

We gratefully acknowledge financial support from the University of Washington.

## ABBREVIATIONS

- 3DP, three-dimensional printing
- CAD, computer aided design
- FFF, fused filament fabrication
- GPC, gel permeation chromatography
- Oct, octoate
- PCL, poly( $\epsilon$ -caprolactone)

## REFERENCES

- (1) Hofmann, M. 3D Printing Gets a Boost and Opportunities with Polymer Materials. *ACS Macro Lett.* **2014**, *3*, 382–386.
- (2) Gross, B. C.; Erkal, J. L.; Lockwood, S. Y.; Chen, C.; Spence, D. M. Evaluation of 3D Printing and Its Potential Impact on Biotechnology and the Chemical Sciences. *Anal. Chem.* **2014**, *86*, 3240–3253.
- (3) Jones, N. The Print Revolution: Three Dimensional Printers Are Opening Up New Worlds to Research. *Nature* **2012**, *487*, 22–23.
- (4) Wang, X.; Guo, Q.; Cai, X.; Zhou, S.; Kobe, B.; Yang, J. Initiator-Integrated 3D Printing Enables the Formation of Complex Metallic Architectures. *ACS Appl. Mater. Interfaces* **2014**, *6*, 2583–2587.
- (5) Bakarich, S. E.; Gorkin, R., III; in het Panhuis, M.; Spinks, G. M. Three-Dimensional Printing Fiber Reinforced Hydrogel Composites. *ACS Appl. Mater. Interfaces* **2014**, *6*, 15998–16006.
- (6) Khaled, S. A.; Burley, J. C.; Alexander, M. R.; Roberts, C. J. Desktop 3D Printing of Controlled Release Pharmaceutical Bilayer Tablets. *Int. J. Pharm.* **2014**, *461*, 105–111.
- (7) Yu, D.-G.; Shen, X.-X.; Branford-White, C.; Zhu, L.-M.; White, K.; Yang, X. L. Novel Oral Fast-Disintegrating Drug Delivery Devices with Predefined Inner Structure Fabricated by Three-Dimensional Printing. *J. Pharm. Pharmacol.* **2009**, *61*, 323–329.

- (8) Derby, B. Printing and Prototyping of Tissues and Scaffolds. *Science* **2012**, *338*, 921–926.
- (9) Melchels, F. P. W.; Domingos, M. A. N.; Klein, T. J.; Malda, J.; Bartolo, P. J.; Hutmacher, D. W. Additive Manufacturing of Tissues and Organs. *Prog. Polym. Sci.* **2012**, *37*, 1079–1104.
- (10) Billiet, T.; Vandenhante, M.; Schelfhout, J.; Van Vlierberghe, S.; Dubrule, P. A Review of Trends and Limitations in Hydrogel-Rapid Prototyping for Tissue Engineering. *Biomaterials* **2012**, *33*, 6020–6041.
- (11) Xu, N.; Ye, X.; Wei, D.; Zhong, J.; Chen, Y.; Xu, G.; He, D. 3D Artificial Bones for Bone Repair Prepared by Computed Tomography-Guided Fused Deposition Modeling for Bone Repair. *ACS Appl. Mater. Interfaces* **2014**, *6*, 14952–14963.
- (12) Zhao, C.; Wang, C.; Gorkin, R., III; Beirne, S.; Shu, K.; Wallace, G. G. Three Dimensional (3D) Printed Electrodes for Interdigitated Supercapacitors. *Electrochem. Commun.* **2014**, *41*, 20–23.
- (13) Sun, K.; Wei, T.-S.; Ahn, B. Y.; Seo, J. Y.; Dillon, S. J.; Lewis, J. A. 3D Printing of Interdigitated Li-Ion Microbattery Architectures. *Adv. Mater.* **2013**, *25*, 4539–4543.
- (14) Manoor, M. S.; Jiang, Z.; James, T.; Kong, Y. L.; Malatesta, K. A.; Soboyejo, W. O.; Verma, N.; Gracias, D. H.; McAlpine, M. C. 3D Printed Bionic Ears. *Nano Lett.* **2013**, *13*, 2634–2639.
- (15) Leigh, S. J.; Bradley, R. J.; Purcell, C. P.; Billson, D. R.; Hutchins, D. A. A Simple, Low-Cost Conductive Composite Material for 3D Printing of Electronic Sensors. *PLoS One* **2012**, *7*, e49365.
- (16) Czyzewski, J.; Burzynski, P.; Gawel, K.; Meisner, J. Rapid Prototyping of Electrically Conductive Components Using 3D Printing Technology. *J. Mater. Process. Technol.* **2009**, *209*, 5281–5285.
- (17) Espalin, D.; Muse, D.; MacDonald, E.; Wicker, R. 3D Printing Multifunctionality: Structure With Electronics. *Int. J. Adv. Manuf. Technol.* **2014**, *72*, 963–978.
- (18) Muth, J. T.; Vogt, D. M.; Truby, R. L.; Menguc, Y.; Kolesky, D. B.; Wood, R. J.; Lewis, J. A. Embedded 3D Printing of Strain Sensors within Highly Stretchable Elastomers. *Adv. Mater.* **2014**, *26*, 6307–6312.
- (19) Kim, K.; Zhu, W.; Qu, X.; Aaranson, C.; McCall, W. R.; Chen, S.; Sirbully, D. J. 3D Optical Printing of Piezoelectric Nanoparticle–Polymer Composite Materials. *ACS Nano* **2014**, *8* (10), 9799–9806.
- (20) Peterson, G. I.; Yurtoglu, M.; Larsen, M. B.; Craig, S. L.; Ganter, M. A.; Storti, D. W.; Boydston, A. J. Additive Manufacturing of Mechanochromic Polycaprolactone on Entry-Level Systems. *Rapid Prototyping J.* **2004**, submitted.
- (21) Wiggins, K. M.; Brantley, J. N.; Bielawski, C. W. Methods for Activating and Characterizing Mechanically Responsive Polymers. *Chem. Soc. Rev.* **2013**, *42*, 7130–7147.
- (22) Brantley, J. N.; Wiggins, K. M.; Bielawski, C. W. Polymer Mechanochemistry: The Design and Study of Mechanoophores. *Polym. Int.* **2012**, *62*, 2–12.
- (23) Caruso, M. M.; Davis, D. A.; Shen, Q.; Odom, S. A.; Sottos, N. R.; White, S. R.; Moore, J. S. Mechanically Induced Chemical Changes in Polymeric Materials. *Chem. Rev.* **2009**, *109*, 5755–5798.
- (24) Beyer, M. K.; Clausen-Schaumann, H. Mechanochemistry: The Mechanical Activation of Covalent Bonds. *Chem. Rev.* **2005**, *105*, 2921–2948.
- (25) Gossweiler, G. R.; Hewage, G. B.; Soriano, G.; Wang, Q.; Welshofer, G. W.; Zhao, X.; Craig, S. L. Mechanochemical Activation of Covalent Bonds in Polymers with Full and Repeatable Macroscopic Shape Recovery. *ACS Macro Lett.* **2014**, *3*, 216–219.
- (26) Grady, M. E.; Beiermann, B. A.; Moore, J. S.; Sottos, N. R. Shockwave Loading of Mechanochemically Active Polymer Coatings. *ACS Appl. Mater. Interfaces* **2014**, *6*, 5350–5355.
- (27) Lee, C. K.; Beiermann, B. A.; Silberstein, M. N.; Wang, J.; Moore, J. S.; Sottos, N. R.; Braun, P. V. Exploiting Force Sensitive Spiropyrans as Molecular Level Probes. *Macromolecules* **2013**, *46*, 3746–3752.
- (28) Beiermann, B. A.; Kramer, S. L. B.; Moore, J. S.; White, S. R.; Sottos, N. R. Role of Mechanoophore Orientation in Mechanochemical Reactions. *ACS Macro Lett.* **2012**, *1*, 163–166.
- (29) O'Bryan, G.; Wong, B. M.; McElhanon, J. R. Stress Sensing in Polycaprolactone Films via an Embedded Photochromic Compound. *ACS Appl. Mater. Interfaces* **2010**, *2*, 1594–1600.
- (30) Davis, D. A.; Hamilton, A.; Yang, J.; Cremar, L. D.; Van Gough, D.; Potisek, S. L.; Ong, M. T.; Braun, P. V.; Martinez, T. J.; White, S. R.; Moore, J. S.; Sottos, N. R. Force-Induced Activation of Covalent Bonds in Mechanoresponsive Polymeric Materials. *Nature* **2009**, *459*, 68–72.
- (31) Chen, Y.; Spiering, A. J. H.; Karthikeyan, S.; Peters, G. W. M.; Meijer, E. W.; Sijbesma, R. P. Mechanically Induced Chemiluminescence from Polymer Incorporating a 1,2-Dioxetane Unit in the Main Chain. *Nat. Chem.* **2012**, *4*, 559–562.
- (32) Ducrot, E.; Chen, Y.; Bulters, M. J. H.; Sijbesma, R. P.; Creton, C. Toughening Elastomers with Sacrificial Bonds and Watching Them Break. *Science* **2014**, *344*, 186–189.
- (33) Jakobs, R. T. M.; Ma, S.; Sijbesma, R. P. Mechanocatalytic Polymerization and Cross-Linking in a Polymeric Matrix. *ACS Macro Lett.* **2013**, *2*, 613–616.
- (34) Black Ramirez, A. L.; Kean, Z. S.; Orlicki, J. A.; Champhekar, M.; Elsakr, S. M.; Krause, W. E.; Craig, S. L. Mechanochemical Strengthening of a Synthetic Polymer in Response to Typically Destructive Shear Forces. *Nat. Chem.* **2013**, *5*, 757–761.
- (35) Larsen, M. B.; Boydston, A. J. Successive Mechanochemical Activation and Small Molecule Release in an Elastomeric Material. *J. Am. Chem. Soc.* **2014**, *136*, 1276–1279.
- (36) Larsen, M. B.; Boydston, A. J. “Flex- Activated” Mechanoophores: Using Polymer Mechanochemistry to Direct Bond Bending Activation. *J. Am. Chem. Soc.* **2013**, *135*, 8189–8192.
- (37) Diesendruck, C. E.; Steinberg, B. D.; Sugai, N.; Silberstein, M. N.; Sottos, N. R.; White, S. R.; Braun, P. V.; Moore, J. S. Proton-Coupled Mechanochemical Transduction: A Mechanogenerated Acid. *J. Am. Chem. Soc.* **2012**, *134*, 12446–12449.
- (38) Raymo, F. M.; Giordani, S. Signal Processing at the Molecular Level. *J. Am. Chem. Soc.* **2001**, *123*, 4651–4652.
- (39) Frédéric, R.; Robert, S.; Charlier, C.; de Ruyck, J.; Wouters, J.; Pirotte, B.; Masereel, B.; Pochet, L. 3,6-Disubstituted Coumarins as mechanism-Based Inhibitors of Thrombin and Factor Xa. *J. Med. Chem.* **2005**, *48*, 7592–7603.
- (40) Eshraghi, S.; Das, S. Mechanical and Microstructural Properties of Polycaprolactone Scaffolds with One-Dimensional, Two-Dimensional, and Three-Dimensional Orthogonally Oriented Porous Architectures Produced by Selective Laser Sintering. *Acta Biomater.* **2010**, *6*, 2467–2476.
- (41) Keum, S.-R.; Lee, K.-B.; Kazmaier, P. K.; Buncel, E. A Novel Method for Measurement of the Merocyanine-Spiropyran Interconversion in Non-Activated 1,3,3-Trimethylspiro-(2H-1-benzopyran-2,2'-indoline) Derivatives. *Tetrahedron Lett.* **1994**, *35*, 1015–1018.
- (42) Keum, S.-R.; Lee, M.-J. Nonactivated Arylazoindolinobenzospiropyran Derivatives. Part 2: Preparation and Kinetic Measurements of the Spiro-ring Formation from the Merocyanine Form. *Bull. Korean Chem. Soc.* **1999**, *20*, 1464–1468.
- (43) Aramaki, S.; Atkinson, G. H. Spironaphthopyran Photochromism: Picosecond Time-Resolved Spectroscopy. *J. Am. Chem. Soc.* **1992**, *114*, 438–444.